MOTION CONTROLLER FOR THE TITAN ROBOTIC MANIPULATOR DEDICATED FOR ON-ORBIT SERVICING OPERATIONS

Tomasz Rybus [(1)], Mateusz Wojtunik [(1)], Filip Dyba [(1)], Kacper Mikołajczyk [(1)], Karol Seweryn [(1)], Roman Wawrzaszek [(1)], Daria Pączkowska [(2)]

1. Centrum Badań Kosmicznych Polskiej Akademii Nauk (CBK PAN), Bartycka 18a, 00-716 Warsaw, Poland, trybus@cbk.waw.pl, mwojtunik@cbk.waw.pl, f.dyba28@gmail.com, kacper.mikolajczyk96@gmail.com, kseweryn@cbk.waw.pl, wawrzasz@cbk.waw.pl

2. PIAP Space, al. Jerozolimskie 202, 02-486 Warsaw, Poland, daria.paczkowska@piap-space.com

ABSTRACT

The TITAN robotic arm is planned as a manipulator designed for on-orbit servicing and debris removal. In this paper, we present a Motion Controller (MC) developed for this manipulator. The MC is a control system responsible for the whole arm control and enables the manipulator to perform capture and servicing tasks. It can operate with varying levels of autonomy and in multiple modes, including compliant control and task-space trajectory tracking. Analytical methods were used to confirm the stability of the control system at the joint level for various parameter sets, while the Monte Carlo method was employed to assess MC stability at the manipulator level. The MC was validated in numerical simulations, which proved that it correctly achieves control task despite variability of scenario parameters.

1. INTRODUCTION

Malfunctions occurring in orbit can shorten the operational lifetime of satellites [1]. A significant number of common failures could potentially be repaired on orbit [2]. Servicing missions carried out by the Space Shuttle, such as the repair of the Solar Max satellite, demonstrated the potential of on-orbit servicing (OOS) [3]. Currently planned OOS missions will rely on the use of unmanned servicing satellites [4]. Such a satellite, often referred to as a "chaser", should be equipped with a robotic manipulator for capturing malfunctioning satellites and performing servicing tasks [5]. It is also proposed to use a manipulator for capturing space debris in active debris removal (ADR) missions [6].

The first ideas for unmanned OOS missions began to appear in the 1980s [7]. The concepts of the Geostationary Servicing Satellite (GSV) [8] and RObotic Geostationary Orbit Restorer (ROGER) [9] were developed as a part of studies funded by the European Space Agency (ESA). Other concepts of OOS missions include Deutsche Orbitale Servicing Mission (DEOS) [10] and ConeXpress Orbital Life Extension Vehicle (CX-OLEV) [11]. The key technologies needed for OOS and ADR have matured through ground testing [12] and orbital demonstration missions such as ETS-VII [13] and Orbital Express [14].

Grasping of the uncontrolled tumbling client satellite will pose the greatest challenge in OOS and ADR missions. In this paper we focus on the problem of controlling the manipulator during in-orbit capture and servicing tasks. The control system must use feedback from the vision system to guide the end-effector of the manipulator to the desired position with respect to the target object [15]. Such control is known as the visual servoing [16]. It is usually proposed to locate the camera on the end-effector and to use Jacobian-based control of the manipulator [17]. Validation of such approach was performed during the ETS-VII orbital mission [13]. The position and orientation of the chaser satellite are affected by the motion of the manipulator. Thus, Umetani and Yoshida introduced the Resolved Motion Rate Control based on the Dynamic Jacobian that takes into account the dynamic coupling between the manipulator and the chaser [18]. In recent years various approaches for visual servoing were proposed and validated, e.g. [19]. The control law should consider the fact that the camera provides measurements of the client satellite state relative to the camera frame [20]. Moreover, the control system of the manipulator should be stable [21]. In addition, compliant control is needed during the contact between the gripper and the target object [22].

In this paper we present a control system developed for the TITAN manipulator in the scope of the project "Robotic Arm Development for On-Orbit Servicing Operations" funded by ESA. This control system, called the Motion Controller (MC), is responsible for the whole arm control and allows the manipulator to perform on-orbit capture and servicing tasks. It can be operated in multiple control modes, including task-space trajectory tracking, compliant control and joint-space control. The presented system can be used with various levels of autonomy. Several practical aspects, such as error handling, are considered. The MC is validated in high-fidelity numerical simulations and its stability is proven on the joint level and on the manipulator level.

The paper is organized as follows. The TITAN manipulator is described in Section 2, while the MC is presented in Section 3. Section 4 contains the stability analysis. Results of the MC validation are shown in Section 5. The conclusions are given in Section 6.

2. TITAN MANIPULATOR

2.1. Manipulator design

The TITAN robotic arm is planned as a redundant 7 Degrees of Freedom (DoF) manipulator dedicated for OOS and ADR missions [23]. It is being developed by a Polish consortium comprising of PIAP Space (the leader of the consortium), Space Research Centre of the Polish Academy of Sciences (CBK PAN) and Spacive. The Denavit–Hartenberg (DH) parameters of the TITAN manipulator are given in Tab. 1. Two types of joints are used: large (joints 1, 2, and 3) and small (joints 4, 5, 6, and 7). The manipulator is equipped with a gripper that can be used for grasping the Launch Adapter Ring (LAR) of the client satellite. Encoders provide measurements of angular positions of manipulator joints. A visual pose estimation system uses data from a camera mounted on the last link of the manipulator to estimate the relative position and orientation of the client satellite with respect to the gripper. A 6 DoF Force/Torque Sensor (FTS) is mounted between the last link and the gripper.

Table 1. DH parameters of the TITAN manipulator.

Joint	θ_i [rad]	λ_i [m]	L_i [m]	α_i [rad]
1	θ_1	0.37	0	$\pi/2$
2	θ_2	0.314	0	$-\pi/2$
3	$\theta_3+\pi$	0.7	0	$\pi/2$
4	θ_4	0.264	0	$-\pi/2$
5	θ_5	0.4	0	$\pi/2$
6	θ_6	0.264	0	$-\pi/2$
7	θ_7	0.5435	0	0

2.2. Dynamics

It is assumed that the TITAN manipulator will be mounted on a relatively small chaser satellite. The control system of the chaser may not be able to fully compensate the reaction forces and torques induced by the manipulator motion [10]. Thus, the chaser's control system is assumed to be turned off during the capture operation. In such a case the satellite-manipulator system is in a free-floating state [24]. The dynamic equations of the system can be presented as follows [25]:

$$\begin{bmatrix} \mathbf{M}_{ch} & \mathbf{M}_{ch/m} \\ \mathbf{M}_{ch/m}^T & \mathbf{M}_m \end{bmatrix} \dot{\mathbf{q}}_v + \begin{bmatrix} \mathbf{C}_{ch} \\ \mathbf{C}_m \end{bmatrix} \mathbf{q}_v = \begin{bmatrix} \mathbf{F}_{ch} \\ \mathbf{T}_{ch} \\ \mathbf{u}_m \end{bmatrix} \quad (1)$$

where $\mathbf{q}_v = [\mathbf{v}_{ch}^T \quad \boldsymbol{\omega}_{ch}^T \quad \dot{\boldsymbol{\theta}}^T]^T$, $\mathbf{v}_{ch}$ and $\boldsymbol{\omega}_{ch}$ are the linear and angular velocity of the chaser, respectively, $\dot{\boldsymbol{\theta}}$ is the angular velocity of manipulator joints, $\mathbf{M}_{ch}$ is the mass matrix of the chaser, $\mathbf{M}_m$ is the mass matrix of the manipulator, while $\mathbf{M}_{ch/m}$ is the mass matrix of the coupling between the chaser and the manipulator, $\mathbf{C}_{ch}$ and $\mathbf{C}_m$ are the Coriolis matrices of the chaser and of the manipulator, respectively, $\mathbf{F}_{ch}$ and $\mathbf{T}_{ch}$ denote the external force and torque acting on the chaser, while $\mathbf{u}_m$ is the vector of control torques applied on the manipulator joints. We assume that during the capture operation $\mathbf{F}_{ch} = \mathbf{T}_{ch} = \mathbf{0}$. As a result, the momentum $\mathbf{P}$ and angular momentum $\mathbf{L}$ of the system are conserved:

$$\begin{bmatrix} \mathbf{P} \\ \mathbf{L} \end{bmatrix} = \mathbf{H}_1 \begin{bmatrix} \mathbf{v}_{ch} \\ \boldsymbol{\omega}_{ch} \end{bmatrix} + \mathbf{H}_2 \dot{\boldsymbol{\theta}} = \begin{bmatrix} \mathbf{0} \\ \mathbf{0} \end{bmatrix} \quad (2)$$

Definition of matrices $\mathbf{M}_{ch}, \mathbf{M}_m, \mathbf{M}_{ch/m}, \mathbf{C}_{ch}, \mathbf{C}_m, \mathbf{H}_1$ and $\mathbf{H}_2$ can be found in [25]. From Eq. (2) we obtain:

$$\begin{bmatrix} \mathbf{v}_{ch} \\ \boldsymbol{\omega}_{ch} \end{bmatrix} = -\mathbf{H}_1{}^{-1}\mathbf{H}_2 \dot{\boldsymbol{\theta}} \quad (3)$$

The linear and angular velocity of the gripper is given by:

$$\begin{bmatrix} \mathbf{v}_g \\ \boldsymbol{\omega}_g \end{bmatrix} = \mathbf{J}_{ch} \begin{bmatrix} \mathbf{v}_{ch} \\ \boldsymbol{\omega}_{ch} \end{bmatrix} + \mathbf{J}_m \dot{\boldsymbol{\theta}} \quad (4)$$

where $\mathbf{J}_{ch}$ and $\mathbf{J}_m$ are the Jacobian matrix of the chaser and Jacobian matrix of the manipulator, respectively. By substituting Eq. (3) into Eq. (4) we obtain the following relation for the linear and angular velocity of the gripper:

$$\begin{bmatrix} \mathbf{v}_g \\ \boldsymbol{\omega}_g \end{bmatrix} = \mathbf{J}_{dyn} \dot{\boldsymbol{\theta}} \quad (5)$$

where $\mathbf{J}_{dyn}$ is the Dynamic Jacobian given by:

$$\mathbf{J}_{dyn} = \mathbf{J}_m - \mathbf{J}_{ch}\mathbf{H}_1{}^{-1}\mathbf{H}_2 \quad (6)$$

3. MOTION CONTROLLER

3.1. General structure

The MC is composed of two modules: the Trajectory Planning Module and the Closed-loop Controller. The first module is responsible for generating feasible trajectory of the manipulator (in the joint space or in the Cartesian space). It could also be used for transmitting the desired manipulator position from the Ground Station (GS). The second module is responsible for the closed-loop control of the manipulator. This control relies on measurements from encoders and the FTS, as well as the estimated pose of the client satellite. Control signal from the Closed-loop Controller is transmitted to the Robotic Arm Controller (RAC), which is responsible for communication with Joint Controllers. The general structure of the MC is shown in Fig. 1.

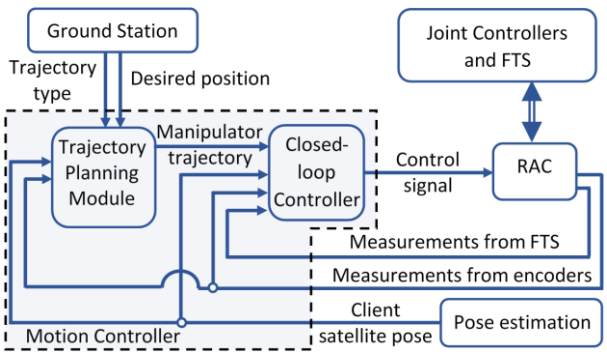

Figure 1. General structure of the MC.

3.2. Control modes and operational scenario

The MC can be operated in eight basic control modes: Braked/Standby mode, Passive mode, Joint Position mode, Joint Velocity mode, Cartesian Control mode, Active 6 DoF Force/Torque Control mode (the compliant control), Direct Drive mode (open loop), and Joint Torque mode. We also distinguish three modes of operation. In the Single Control Mode Execution the MC executes one commanded control mode. It is applicable to a single operation with fully defined initial condition. In the Interactive Autonomy mode the MC executes a pre-planned automatic mission sequences. The fully autonomous capture manoeuvre (that includes approach, capture of the client and docking) is realized on the mission level. In such a case the MC works under the supervision of the chaser control system.

The nominal scenario is defined as follows. During the orbital rendezvous the manipulator is deployed with the use of the Joint Position mode. The chaser satellite is in synchronous flight with the client satellite. After the final positioning of the chaser the Point of Resolution (POR) of the gripper reaches the point that is 0.3 m away from the LAR of the client. The chaser enters free drift (satellite control is turned off) and the capture manoeuvre begins with the manipulator approach phase. The manipulator is controlled using the Cartesian Control mode with the feedback from the pose estimation system in order to reach close proximity of the LAR. When the POR is considered to be 0.05 m away from the LAR, the control mode is switched to the Active 6 DoF Force/Torque Control mode (detailed description of this control can be found in [26]). As compensation of the initial forces and torques acting on the gripper might be necessary, this control is turned on before the first contact with the LAR. During the grasping phase the manipulator can be controlled with the Active 6 DoF Force/Torque Control mode or with the Passive mode. After the connection between the gripper and the LAR is rigidized, the Joint Velocity mode is used for braking in order to ensure zero angular velocities of the manipulator's joints. Subsequently, the manipulator is moved to a docking configuration. Afterwards, the servicing operations can be performed with the use of the Cartesian Control mode or the Active 6 DoF Force/Torque Control mode.

3.3. Cartesian Control mode

In this mode the MC is maintaining/tracking the position and orientation of the POR described in the Cartesian space based on the commanded set-point. The Jacobian matrix representing the relationship between the joint space and the Cartesian space velocities is used to solve the inverse kinematics problem. One of two variants of the control law can be used: one is based on the Kinematic Jacobian $\mathbf{J}_m$, while the other is based on the Dynamic Jacobian $\mathbf{J}_{dyn}$ that is calculated using the dynamic parameters of the system (the chaser and the manipulator). This allows to predict the influence of the manipulator motion on the free-floating base and to achieve better compensation of the POR position and orientation error. In the Cartesian Control mode based on $\mathbf{J}_{dyn}$, the desired velocities of manipulator joints are calculated with the following control law:

$$\left(\dot{\boldsymbol{\theta}}\right)_{des} = \left(\mathbf{J}_{dyn}^{(POR)}(\boldsymbol{\theta})\right)^{\#} \mathbf{G} \begin{bmatrix} \left(\mathbf{p}_{POR}^{(LAR)}\right)_{des} - \mathbf{p}_{POR}^{(LAR)} \\ \left(\boldsymbol{\epsilon}_{POR}^{(LAR)}\right)_{des} - \boldsymbol{\epsilon}_{POR}^{(LAR)} \end{bmatrix} \quad (7)$$

where $\boldsymbol{\theta}$ is the angular position of manipulator joints, $\mathbf{p}_{POR}$ is the position of the POR, while $\boldsymbol{\epsilon}_{POR}$ is a unit quaternion that describes the orientation of the POR, the subscript des denotes the desired value, the superscript in brackets indicates the frame in which the given variable is expressed (the LAR frame or the POR frame), # denotes the Moore-Penrose pseudoinverse of a matrix, while $\mathbf{G}$ denotes the gain matrix defined as:

$$\mathbf{G} = \begin{bmatrix} \mathbf{Rot}_{LAR}^{POR}\mathbf{K}_{lin} & \mathbf{0}_{3\times4} \\ \mathbf{0}_{3\times3} & \mathbf{Rot}_{LAR}^{POR}\mathbf{T}_{qtn}^{\#}\mathbf{K}_{qtn} \end{bmatrix} \quad (8)$$

where $\mathbf{Rot}_{LAR}^{POR}$ is the rotation matrix describing orientation of the LAR with respect to the POR, $\mathbf{T}_{qtn}$ transforms the angular velocity into the time derivative of unit quaternion, $\mathbf{K}_{lin}$ is a 3x3 diagonal positive-definite gain matrix used to convert the position error into the linear velocity, while $\mathbf{K}_{qtn}$ is a 4x4 diagonal positive-definite gain matrix used to calculate the desired time derivative of the POR quaternion.

The desired velocities of the manipulator joints, obtained from Eq. (7), are analysed by the Joint Safety Module. This module guarantees that trajectories of the desired joint angular velocities, generated by the MC, do not exceed the defined limitations for joint angular velocities and accelerations. Subsequently, the desired joint angular velocities are transmitted through the RAC to the Joint Controllers, which utilize Field Oriented Control (FOC) to ensure that these velocities are achieved. The diagram of the Cartesian Control mode is shown in Fig. 2.

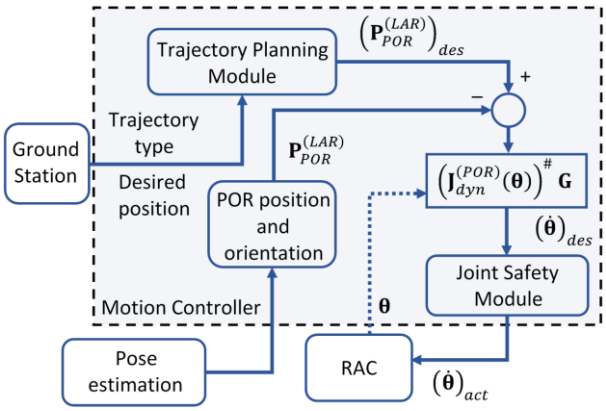

Figure 2. Closed-loop control in the Cartesian control mode based on the Dynamic Jacobian.

3.4. Null-space control

Null-space control can be used in the Cartesian Control mode and Active 6-DoF Force/Torque Control mode to take advantage of the manipulator's kinematic redundancy [27]. The minimal representation of the Cartesian space POR velocity (linear and angular) requires 6 independent variables, while the TITAN manipulator has 7 DoF. Thus, there is an infinite number of joint space velocities corresponding to a given Cartesian space POR velocity. For every joint space position, kinematically redundant manipulator allows to define joint space velocity that does not affect the POR spatial velocity. As a result, an additional task can be fulfilled. When the null-space control is applied, the desired joint velocity profile is defined as follows:

$$(\dot{\boldsymbol{\theta}})_{des} = (\dot{\boldsymbol{\theta}})_{jac} + (\dot{\boldsymbol{\theta}})_{null} \tag{9}$$

where the subscript *jac* indicates the joint space velocity calculated by using the control law based on the Jacobian matrix (Eq. (7)), while the subscript *null* indicates the null-space joint velocity defined as:

$$\dot{\boldsymbol{\theta}}_{null} = -\mathbf{W}(\boldsymbol{\theta}) k_H \nabla \mathrm{H}(\boldsymbol{\theta}) \tag{10}$$

where $\nabla \mathrm{H}(\boldsymbol{\theta})$ is the gradient of the defined cost function, k_H is the scalar positive gain, and $\mathbf{W}(\boldsymbol{\theta})$ is the orthogonal projection matrix onto null-space of the Jacobian matrix.

Three variants of the null-space control are used by the MC: (i) arbitrary joint position tracking (cost function allows minimization of the joint space distance from an arbitrarily defined comfortable pose), (ii) singularity avoidance (cost function allows maximization of the manipulator dexterity), and (iii) self-collision avoidance (when the shortest distance between two links is smaller than the defined activation distance, the motion of joints that results from the null-space control will move the links away from each other, increasing the shortest distance). It is noteworthy that the cost functions are additive. Thus, all of the variants can be used at once with gains that strengthen or weaken the specific task of the null-space control.

3.5. Error Handling

During autonomous operations, the MC is responsible for error handling. The MC reacts to the critical and non-critical errors detected during the operation. If the MC detects a critical error, it autonomously decides to abort the operation and stops the manipulator motion by issuing 0 joint velocity command. Critical errors may arise in the following scenarios: data loss from the pose estimation system or the RAC due to connection time-outs, joint positions evaluated by the Joint Safety Module exceeding defined limits, joint positions or velocities received from the RAC exceeding defined limits, commanded joint positions (in the Joint Position mode) or velocities (in the Joint Velocity mode) exceeding defined limits, excessive forces or torques measured by the FTS, manipulability index falling below the specified tolerance (indicating proximity to a singularity or workspace boundary), or the distance between the two manipulator links being less than the given tolerance (a potential self-collision pose).

4. STABILITY ANALYSIS

Due to the fact that the manipulator mounted on the chaser is a nonholonomic system, there is no straightforward way to perform linearization of the system in order to analyze stability of the control system using analytical methods [28]. Therefore, analytical stability analysis was performed for the independent Joint Controller system, while the stability analysis of the MC is performed via the Monte Carlo campaign.

4.1. Joint level stability

The Joint Controller is responsible for executing the desired velocity of manipulator joints generated by the MC. The stability of the joint velocity loop is analysed analytically using an independent joint model. It's a common practice to assess stability margins for free-floating manipulators based on independent joint models [29]. The joint model is nonlinear and have to be linearized in order to use the Nyquist theory to assess stability margins. The system consists of the Joint Controller software (velocity loop), electronic part dynamics and mechanical part dynamics. The schematic view of the considered joint model is presented in Fig. 3. The Electrical system block consists of multiple, nonlinear parts that are hard to model and linearize. Therefore, this subsystem is modelled as a linear 1st-order system. The mechanical part consists of the fast rotating motor, gear and slowly rotating link. The following aspects are taken into consideration: gear efficiency, control signal saturation, joint flexibility, joint viscous friction and external load.

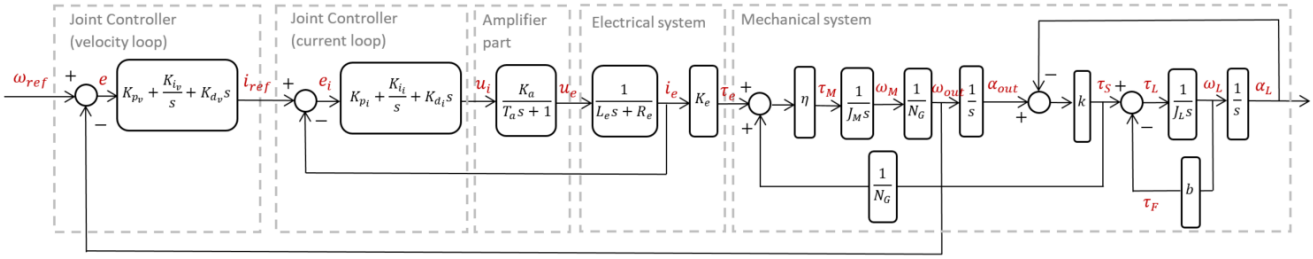

Figure 3. Linearized model used for Joint Controller stability analysis – Joint Velocity control mode.

The final open-loop transfer function of the Joint Controller model operated in the velocity loop is given as:

$$G_{o_V} = \frac{\omega_{out}}{e_\omega} = \frac{G_v}{G_{2_v} + G_{3_v}} \tag{11}$$

where:

$$G_v = K_{p_v} + \frac{K_{i_v}}{s} + K_{d_v} s \tag{12}$$

$$G_{2_v} = \frac{G_{1_v} J_M N_G s}{K_e \eta} - \frac{G_{1_v} k}{K_e N_G s} \tag{13}$$

$$G_{3_v} = \frac{G_{1_v} k}{K_e N_G} \frac{k}{J_L s^3 + b s^2 + k s} \tag{14}$$

$$G_{1_v} = 1 + \frac{(T_a s + 1)(L_e s + R_e)}{G_i K_a} \tag{15}$$

$$G_i = K_{p_i} + \frac{K_{i_i}}{s} + K_{d_i} s \tag{16}$$

In the above equations ω_{out} denotes the angular velocity of the output shaft of the gear, e_ω denotes the joint velocity error, s is the Laplace argument, K_{p_v}, K_{i_v} and K_{d_v} represent the proportional, integral and derivative gains of the velocity loop controller, while K_{p_i}, K_{i_i} and K_{d_i} represent the proportional, integral and derivative gains of the current loop controller, K_a and T_a are the amplifier gain and time constant, respectively, L_e, R_e and K_e are the motor inductance, resistance and torque constant, respectively, N_G denotes the gear reduction ratio, while η denotes the gear efficiency, k is the spring constant, b represents the viscous damping (friction) constant, J_M is the motor inertia and J_L is the link inertia.

The transfer function given in Eq. (11) can be directly used to assess the stability margins. The Monte Carlo method was introduced in the simulation studies to verify the model robustness to chosen model parameters. Four parameters were randomized: gearbox stiffness, link inertia, viscous damping coefficient and gear efficiency. These values are not constant in the real system, therefore in the linearized model different sets of parameters were chosen and stability properties as well as control performance measures were evaluated. Small and large manipulator joints were evaluated separately. In this section we present results obtained for a large joint. The Bode plots for 98 Monte Carlo runs are shown in Fig. 4, while step and impulse response is presented in Fig. 5. The requirement for stability margins was fulfilled in 97 out of 98 runs. In one run the Joint Controller was stable, but the stability margins did not meet the requirement. The average overshoot of the step response from the Monte Carlo runs was much higher than the one obtained for nominal system parameters (the maximal overshoot is 43.3 %). The settling time of the step response varies in dependence of randomized set. The lowest value equals 1.34 s, while the maximum value equals 32.96 s.

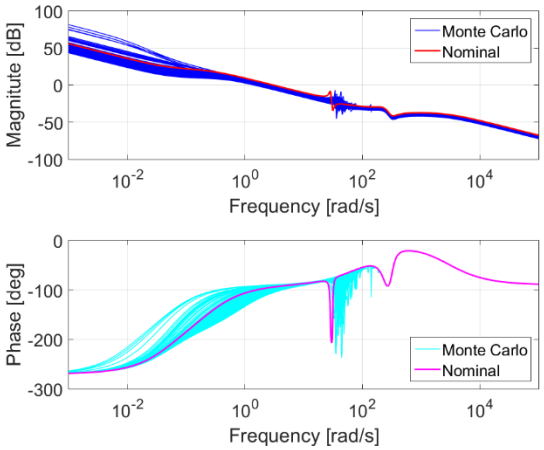

Figure 4. Bode plots obtained for a large joint.

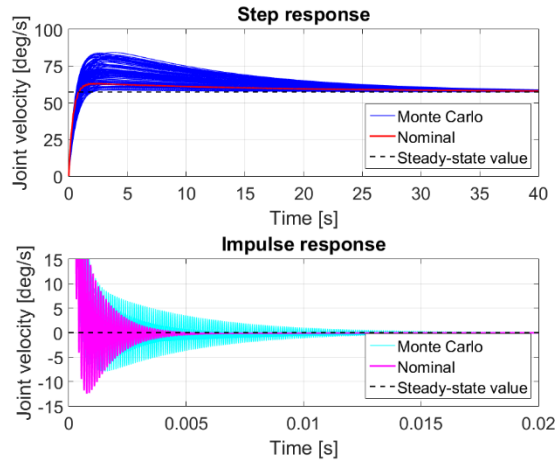

Figure 5. Step and impulse response for a large joint.

4.2. Manipulator level stability

The Monte Carlo analysis was performed in order to assess the stability of the MC in the Cartesian Control mode on the manipulator level. In the considered scenario this control mode was used to drive the POR of the gripper to the LAR of the client satellite. The analysis was performed for a non-moving client satellite, because it is not possible to assess the stability of the control system in case of moving desired point (there is no straightforward way to distinguish if the control system is unstable or simply too slow to reach the moving point). In each run, the initial conditions of the system were randomized so that different scenarios (including the worst case) were analysed in terms of stability. The range of variability of the initial configuration of the manipulator was set to ± 10 deg from the nominal configuration: $\theta_1 = 25.3$ deg, $\theta_2 = 64.3$ deg, $\theta_3 = -82.9$ deg, $\theta_4 = -90.5$ deg, $\theta_5 = 64.3$ deg, $\theta_6 = 96.5$ deg, and $\theta_7 = 62.1$ deg. The initial position and orientation of the client satellite were randomly selected from range of ± 0.1 m from the nominal position in each axis and ± 10 deg from the nominal orientation in each Euler angle. The initial Manipulator joint velocities were

set to zero. The trajectory was planned as 20 second motion, while additional 10 seconds were allocated for keeping the constant desired relative position of the POR with respect to the LAR. 100 Monte Carlo runs were evaluated. The obtained results are shown in Fig. 6. Control errors converge to zero, which indicates that the MC is asymptotically stable.

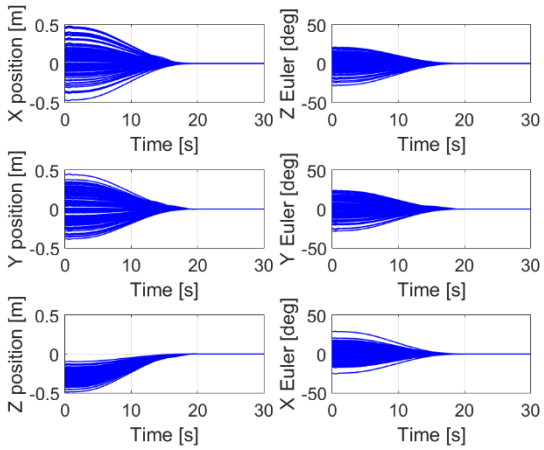

Figure 6. MC stability analysis for the Cartesian Control mode – position and orientation of the POR with respect to the LAR frame.

5. MOTION CONTROLLER VALIDATION

The MC was validated in numerical simulations using the Monte Carlo method. The entire capture operation was considered, but the contact between the gripper and the LAR was neglected due to computational complexity of the contact model (behaviour of the system during the contact was analysed separately). A single simulation was divided into three main phases: (i) the POR follows a trajectory in the Cartesian space and approaches the LAR, (ii) joint braking is performed until the norm of the joint angular velocity vector is below a certain threshold, and (iii) the client satellite is transferred to a certain docking position defined in the joint space. The first phase begins with the Cartesian Control mode. When the POR is in close proximity (0.05 m) to the LAR the control is switched to the Active 6 DoF Force/Torque Control mode. The trajectory in the first phase was planned for 20 seconds. In the second phase all joints are being stopped by commanding zero angular velocities with the use of the Joint Velocity mode. During the first 25% of the maximal time of this phase (3 seconds) joint velocities are reduced by following planned trajectories. Subsequently, constant zero value is defined as the desired one. Such an approach allows to change velocities smoothly and reduce generated joint torques. The duration of this phase may vary depending on the initial condition of the scenario. The Joint Position mode is used in the last phase, which lasts for 200 seconds.

The considered scenario assumes that at the beginning the LAR point on the client satellite, where the local frame associated with the POR should be positioned, is located 0.3 m above the gripper in Z axis direction. In other directions there is no position error between the POR and the LAR. Also, their orientation is identical. The aim of the conducted simulations was to test the MC for a wide range of randomly chosen initial conditions of the on-orbit mission scenario. Thus, the initial linear and angular velocity of the client satellite were randomly chosen with uniform distribution from the following range (with the main axis also chosen randomly): $v_m \in \langle -0.02\ \mathrm{m/s}\,;\,0.02\ \mathrm{m/s}\rangle$ for the main axis of motion and $v_o \in \langle -0.005\ \mathrm{m/s}\,;\,0.005\ \mathrm{m/s}\rangle$ for other axes, while $\omega_m \in \langle -0.9\ \mathrm{deg/s}\,;\,0.9\ \mathrm{deg/s}\rangle$ for the main axis and $\omega_o \in \langle -0.3\ \mathrm{deg/s}\,;\,0.3\ \mathrm{deg/s}\rangle$ for other axes. Random noise was added to the simulated measurements from the visual pose estimation system (± 0.005 m and ± 1 deg for the position and orientation measurements, respectively). The simulations were performed separately for 6 different initial manipulator configurations. For each configuration there were 100 Monte Carlo runs and 7 additional simulations with specific pre-defined initial conditions. The results for all initial configurations are similar in both qualitative and quantitative manner. In this section we present results obtained for the same initial configuration as the one used for the stability analysis in Section 4.2. Frames from animation presenting the capture operation are shown in Fig. 7, on which the chaser is represented as a blue rectangular prism with a hexagonal base. The trajectory of the POR is shown as a solid line. Gripper trajectory tracking error during the first phase of the capture operation (Cartesian Control mode and Active 6 DoF Force/Torque Control mode) is presented in Fig. 8. The maximal values of control torques applied in manipulator joints are given in Tab. 2. The conducted simulations showed high-quality control performance of the MC in various control modes. The entire capture operation was successfully performed in 91 out of 107 simulations. In the remaining simulations, critical errors occurred and the operation had to be aborted by emergency brake of the manipulator.

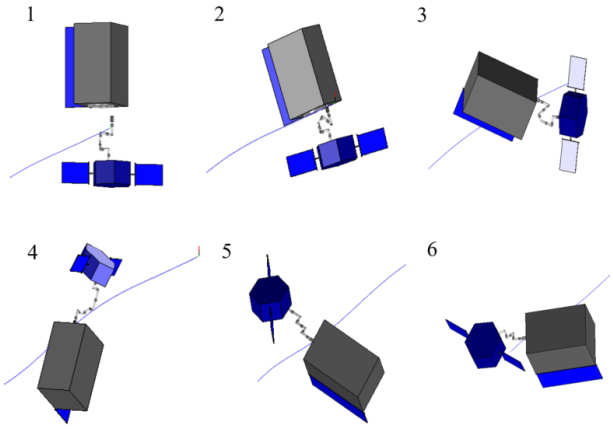

Figure 7. Frames from animation presenting the capture operation.

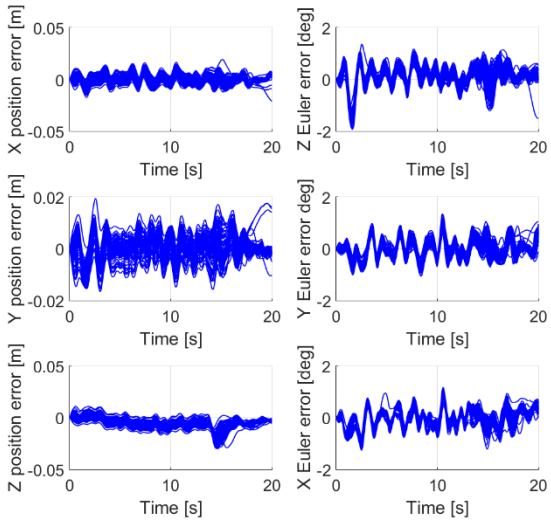

Figure 8. Gripper trajectory tracking error during the first phase of the capture operation.

Table 2. Maximum joint torques.

Joint	Phase 1 [Nm]	Phase 2 [Nm]	Phase 3 [Nm]
1	3.68	4.10	0.46
2	5.22	5.74	0.80
3	2.59	2.26	1.01
4	2.58	4.05	1.27
5	1.98	4.91	1.18
6	0.74	4.95	1.29
7	0.33	2.03	0.65

A position error of 0.03 m in X and Z axes directions, a position error of 0.02 m in Y axis direction and an orientation error of 2 deg in each direction at the end of the first phase of the capture operation correspond with the parameters of the gripper capture envelope and are considered to be acceptable. The main reason of the unsuccessful operations was inaccurate positioning in the capture envelope, which usually resulted from the motion of the client satellite. For some initial velocities the client satellite leaves the manipulator workspace before the POR can be positioned on the LAR. The possibility to correctly perform the capture operation highly depends on the initial manipulator configuration and the initial velocity of the client satellite with respect to the chaser. The highest reaction forces and torques were measured in the braking phase. High loads were observed despite the usage of the polynomial trajectory planning for the Joint Velocity mode. This is caused by high joint angular velocities at the end of the first phase and very short time of the breaking phase. The positioning of the client satellite in the third phase of the capture operation was performed with very low velocities of the manipulator joints in order to reduce loads. As a result, measured values of loads were low despite the fact that the client satellite was rigidly connected to the gripper.

6. CONCLUSIONS

The MC developed for the TITAN manipulator will allow control of the robotic arm during OOS and ADR missions. The MC is responsible for trajectory planning and closed-loop control of the manipulator motion. It can be operated in several control modes, including the Cartesian Control mode and compliant control. One of the variants of the control law is based on the Dynamic Jacobian which takes into account the free-floating nature of the satellite-manipulator system during the capture operation. Analytical analysis allowed to confirm that the control system on the joint level remains stable for various sets of parameters. The Monte Carlo method allowed the assessment of the MC stability on the manipulator level and its robustness to model parameters. Finally, the MC was validated in numerical simulations, in which the entire capture operation was considered. The Monte Carlo simulation campaign has proven that the MC correctly achieves control task despite variability of scenario parameters and fulfils all defined requirements. Maximum values of control torques, loads and angular velocities were evaluated. They did not exceed the defined limits. PIAP Space is working on hardware implementation of the Motion Controller.

7. ACKNOWLEDGMENTS

This paper was partially supported by the European Space Agency project name: Robotic Arm Development For On-Orbit Servicing Operations (TITAN), contract no. 4000131444/20/NL/RA.

8. REFERENCES

1. Ellery, A., Kreisel, J. & Sommer, B. (2008). The case for robotic on-orbit servicing of spacecraft: Spacecraft reliability is a myth. *Acta Astronaut.* **63**(5-6), 632-648.

2. Tafazoli, M. (2009). A study of on-orbit spacecraft failures. *Acta Astronaut.*, **64**(2-3), 195-205.

3. Goodman, J. L. (2006). History of space shuttle rendezvous and proximity operations. *J. Spacecr. Rockets* **43**(5), 944-959.

4. Ma, B., Jiang, Z., Liu, Y. & Xie, Z. (2023). Advances in space robots for on-orbit servicing: A comprehensive review. *Adv. Intell. Syst.* **5**, 2200397.

5. Papadopoulos, E., Aghili, F., Ma, O. & Lampariello, R. (2021). Robotic manipulation and capture in space: A survey. *Front. Robot. AI* **8**, 686723.

6. Ellery, A. (2019). Tutorial review on space manipulators for space debris mitigation. *Robotics* **8**(2), 34.

7. Miller, R.H., Minsky, M.L. & Smith, D.B. (1982). Space applications of Automation, Robotics and

Machine Intelligence Systems (ARAMIS). *NASA Technical Report*, NASA-CR-162082-V0L-4.

8. Yasaka, T. & Ashford, E.W. (1996). GSV - An approach toward space system servicing. *Earth Space Rev.* **5**(2), 9-17.
9. Bischof, B. (2003). ROGER - Robotic Geostationary Orbit Restorer. In *Proc. 54th International Astronautical Congress (IAC'2003)*, Bremen, Germany.
10. Rank, P., Mühlbauer, Q., Naumann, W. & Landzettel, K. (2011). The DEOS automation and robotics payload. In *Proc. 11th ESA Symposium on Advanced Space Technologies in Robotics and Automation (ASTRA'2011)*, Noordwijk, The Netherlands.
11. Del Cura, J.M., Saavedra, G., Sánchez-Maestro, R., Sebastián, A., Tarabini, L. & Ortega, G. (2006). Conexpress Orbital Life Extension Vehicle Cx-Olev Gnc. In: *Proc. 6th International ESA Conference on Guidance, Navigation and Control Systems*, Loutraki, Greece.
12. Wilde, M., Clark, C. & Romano, M. (2019). Historical survey of kinematic and dynamic spacecraft simulators for laboratory experimentation of on-orbit proximity maneuvers. *Prog. Aerosp. Sci.* **110**, 100552.
13. Inaba, N. & Oda, M. (2000). Autonomous satellite capture by a space robot: world first on-orbit experiment on a Japanese robot satellite ETS-VII. In *Proc. 17th IEEE International Conference on Robotics and Automation (ICRA'2000)*, San Francisco, CA, USA.
14. Ogilvie, A., Allport, J., Hannah, M. & Lymer, J. (2008). Autonomous satellite servicing using the orbital express demonstration manipulator system. In *Proc. 9th International Symposium on Artificial Intelligence, Robotics and Automation in Space (i-SAIRAS'2008)*, Los Angeles, CA, USA.
15. Aghili, F. & Parsa, K. (2008). An adaptive vision system for guidance of a robotic manipulator to capture a tumbling satellite with unknown dynamics. In *Proc. 2008 IEEE/RSJ International Conference on Intelligent Robots and Systems (IROS'2008)*, Nice, France.
16. Alepuz, J.P., Emami, M.R. & Pomares, J. (2016). Direct image-based visual servoing of free-floating space manipulators. *Aerosp. Sci. Technol.* **55**, 1-9.
17. Wang, H. & Xie, Y. (2012). Prediction error based adaptive Jacobian tracking for free-floating space manipulators. *IEEE Trans. Aerosp. Electron. Syst.* **48**(4), 3207-3221.
18. Umetani, Y. & Yoshida, K. (1989). Resolved motion rate control of space manipulators with generalized Jacobian matrix. *IEEE Trans. Robot. Autom.* **5**(3), 303-314.
19. Yang, H., Jin, M., Xie, Z., Sun, K. & Liu, H. (2014). Ground verification of space robot capturing the free-floating target based on visual servoing control with time delay. *Ind. Rob.* **41**(6), 543-556.
20. Isenberg, D.R. (2015). Target rendezvous with a space robot using relative position and attitude measurements. In *Proc. IEEE SoutheastCon 2015*, Fort Lauderdale, FL, USA.
21. Wang, H., Guo, D., Xu, H., Chen, W., Liu, T. & Leang, K.K. (2017). Eye-in-hand tracking control of a free-floating space manipulator. *IEEE Trans. Aerosp. Electron. Syst.* **53**(4), 1855-1865.
22. Lampariello, R., Mishra, H., Oumer, N., Schmidt, P., De Stefano, M. & Albu-Schäffer, A. (2018). Tracking control for the grasping of a tumbling satellite with a free-floating robot. *IEEE Robot. Autom. Lett.* **3**(4), 3638-3645.
23. Brzęczkowski, P., Cichorek, K., Darakchiev, R., Kamiński, F., Kleszczyński, D., et al. (2023). TITAN – Development of self-lifting manipulator for on-orbit servicing and debris removal. In *Proc. 17th ESA Symposium on Advanced Space Technologies in Robotics and Automation (ASTRA'2023)*, Leiden, The Netherlands.
24. Dubowsky, S. & Papadopoulos, E. (1993). The kinematics, dynamics, and control of free-flying and free-floating space robotic systems. *IEEE Trans. Robot. Autom.* **9**(5), 531-543.
25. Rybus, T., Wojtunik, M. & Basmadji, F.L. (2022). Optimal collision-free path planning of a free-floating space robot using spline-based trajectories. *Acta Astronaut.* **190**, 395-408.
26. Dyba, F., Rybus, T., Wojtunik, M. & Basmadji, F.L. (2023). Active 6 DoF force/torque control based on Dynamic Jacobian for free-floating space manipulator. *Artificial Satellites: Journal of Planetary Geodesy*, **58**(SI1).
27. Chiaverini, S., Oriolo, G., & Maciejewski, A. A. (2016). Redundant Robots. In *Springer Handbook of Robotics* (Eds. B. Siciliano & O. Khatib). Springer, Cham, pp221-242.
28. Siciliano, B., Sciavicco, L., Villani, L. & Oriolo, G. (2009). *Robotics Modelling, Planning and Control*. Springer-Verlag, London.
29. Ravindran, R. & Doetsch, K. (1982). Design aspects of the shuttle remote manipulator control. In *Proc. Guidance and Control Conference*, San Diego, CA, USA.